Peter Werner, Nikolai D. Zakharov, Gerhard Gerth, Luise Schubert, Ulrich Gösele
MPI für Mikrostrukturphysik, Halle (Saale), Germany

On the formation of Si nanowires by molecular beam epitaxy

Dedicated to Professor Dr. Knut Urban on the occasion of his 65th birthday

Silicon nanowires can be successfully grown by applying the vapor–liquid–solid process. In the case of the commonly used chemical vapor deposition technique, a Si containing gas/precursor is cracked at Au droplets acting as seeds. Si adatoms are subsequently dissolved in the liquid metal. Due to a supersaturation within this droplet, Si precipitates predominantly at the liquid–solid interface – a nanowire grows. A different situation occurs if nanowires are grown by molecular beam epitaxy via the vapor–liquid–solid mechanism. The difference consists, for example, of the role of the metal seed, the morphology of the nanowires and their aspect ratio. In particular, surface diffusion including the metal used as well as Si, strongly influences the growth process. This article describes molecular beam epitaxy growth experiments of Si nanowires under ultra-high vacuum conditions and compares the results with other growth techniques.

Keywords: Semiconductor nanostructure; Silicon nanowires; Molecular beam epitaxy

1. Introduction

During recent years interest in the growth of small nanowhiskers or nanotubes has increased because of their novel electronic, optoelectronic and thermoelectric properties [1–4]. Extensive investigations into the vapor–liquid–solid (VLS) growth of silicon and other materials started in the 1960's [5–8]. However, their fabrication with defined radius, position and length, and their technological applications proved elusive at the time.

Silicon nanowires (NWs) can be synthesized by different techniques: by chemical vapor deposition (CVD) [9–12], by gas-source molecular beam epitaxy (GS-MBE) [13–16], by laser ablation (PLD) [17], by phase decomposition of silicon monoxide [18], and by metal–organic vapor phase epitaxy (MOVPE) [19, 20]. As a further technique, molecular beam epitaxy (MBE) under ultra-high vacuum (UHV) conditions has been applied recently [21], although mainly for the synthesis of compound semiconductor NWs [22].

All these techniques are based on the VLS concept. In its classical concept, small metal clusters, in particular gold droplets, act as a seed to initiate and later to continue the wire growth. When applying a CVD growth technique, the metal particles act as a catalyst, where the precursor gas is dissociated. Only at such singular spots are free semiconductor atoms, such as silicon, generated. They are immediately incorporated into the metal droplet. Due to a supersaturation of the dissolved Si atoms in the liquid droplet, Si atoms precipitate at the liquid–solid interface – the wire grows. Its diameter is determined by the size of the droplet. From a microscopic point of view, two mechanisms are possible: i) layer growth by steps of monolayer height, ii) growth of small crystals at the interface. In this general picture we have to consider that Au and Si form an alloy which contains a eutectic point in the phase diagram at about 360 °C with 19 at.% Si. According to our growth conditions, we worked at the Si-rich branch of the phase diagram. In the following the Au : Si droplets are referred to simply as droplets.

In the case of CVD growth we also have to consider that the precursor is not significantly cracked at the substrate surface. This, therefore, prevents the incorporation of Si atoms; significant growth does not occur at such regions, which represent the majority of the surface. Since CVD reactors work at pressures between 0.1 mbar and 10^3 mbar, the surface is covered with gas molecules. This prevents significant surface diffusion of Si adatoms, even though the substrate temperature is about 300 K higher than for MBE growth.

In the case of the MBE growth, the formation of NWs is also initiated at the metal clusters or droplets. However, there are remarkable differences between NW growth by MBE and growth by those techniques mentioned above.

The substrate surface: Since the nominal pressure in a MBE-UHV chamber lies in the region of 10^{-10} mbar, the growth surface is free of adsorbates of the atmosphere/vapor. If the substrate surface is additionally cleaned by a thermal treatment and, therefore, free of any oxide layer, a temperature-related reconstruction of the Si surface atoms is formed. For example, in our experiments on <111> oriented Si substrates described here, a (7×7) reconstruction is formed.

Si deposition: Due to the electron-beam evaporation used, the flux of the growing species, e. g. Si, consists of single semiconductor atoms. The atoms, which have a specific kinetic energy, directly impinge on the surface. These adatoms may diffuse on the clean Si wafer surface for a specific time before their incorporation. Thus, the surface remains reconstructed as described. The situation changes when one or several Ångström of Au (or any other metal) are deposited first. Then the Si surface is modified by a surface reconstruction including Au and Si atoms (e. g. $\sqrt{3} \times \sqrt{3}$ on (111) surfaces (see below)).

With respect to the relatively low growth temperatures (around 500 °C) applied in our experiments, we assume that

© 2006 Carl Hanser Verlag, Munich, Germany www.ijmr.de Not for use in internet or intranet sites. Not for electronic distribution.

all Si atoms impinging on the surface (on the wafer as well as on Au droplets) are adsorbed; desorbtion can be neglected in this specific case.

Seeding: To get the seeding clusters, a thin metal film is normally deposited and annealed. The substrate surface is thereby i) modified and ii) metal clusters/droplets are formed. The size and shape of these droplets depends on the Si–Au interface energy and the surface energies of the system. Macroscopically this is described by the differences of the chemical potentials (μ_i) at the specific interfaces. The MBE technique allows the formation of seeds and the subsequent NW growth in situ.

Since not much has been reported on the MBE growth of Si NW, especially under UHV conditions, it is the aim of this paper to study the growth phenomena for the generation of Si NWs by this technique. For our investigation, we decided to use small gold clusters as seeds to initiate the formation of the Si NWs. It is possible to use clusters of other metals and alloys, however, gold shows the best properties for a VLS process. Two reasons should be mentioned. First, small islands/droplets can be formed with diameters in the region of up to 400 nm, and second, the existence of a Au : Si alloy allows us to work at lower growth temperatures, quite a lot lower than used for CVD growth (sometimes even below eutectic temperatures, especially for SiGe heterostructure NWs).

Therefore, the first part of the experiments described in this paper deals with the formation of droplets for the subsequent NW growth. We have to take into consideration, in particular, the temperature dependence of the cluster/substrate morphology as well as a modification of the surface of the Si substrate. As will be demonstrated, the Au droplets have a specific size distribution, which is modified by Ostwald ripening dependent on temperature and time.

The second part of the paper is focused on the initial period of the MBE NW growth. Concerning the CVD technique, Si NW formation could be investigated in situ by transmission electron microscopy (TEM) [23]. For our MBE growth studies, TEM facilities were not available, that could guarantee, e. g., a clean surface and a UHV better than 10^{-9} mbar during Si deposition. Therefore, the different growth stages were separately analyzed by scanning electron microscopy (SEM) and TEM after removing the samples from the MBE chamber. The corresponding cooling of the samples might change the droplet/interface structure and has to be taken into account in the subsequent discussion of the experimental results. At this point we also have to check whether there is still a continuous ripening of the Au droplets at the top of the NWs at their initial stages of growth. As will be demonstrated, this has an influence on the NW morphology.

The third part describes NW growth for longer Si deposition times. We will show that, in the case of MBE, the relationship between the lengths and the diameters of the wires behaves differently from the case of CVD- or PLD- generated NW. This has already been reported in a letter by the authors [24]; here we will present this phenomenon in more detail.

2. Experimental

The MBE growth experiments were carried out in a UHV system RIBER SIVA 45, characterized by a base pressure of about 2×10^{-10} mbar. The following evaporation sources were available: three electron-beam evaporation guns for Si, Ge and Au, and effusion cells for dopants such as Sb, In and B. The evaporation rates of Si and Ge were measured and controlled by quadrupole mass spectrometers and corresponding regulation systems. The deposition of Au was monitored by a quartz oscillator.

In all experiments the Si rate was kept constant at 0.05 nm s^{-1}. The flux fluctuations were below 5 % of the total rate. This is important for the comparison and interpretation of the results. The actual substrate temperature T_S was measured indirectly by a thermocouple (W–Re) located between the heater and the substrate. The values were calibrated with a thermocouple welded in the center of the Si wafer to get correct substrate temperatures, T_S (error ± 10 K).

For all experiments 5″ n-type {111} Si wafers were used (As doped, resistivity < 0.005 Ωcm). First, the Si wafers were chemically cleaned by the standard RCA procedure. As a second step, the wafers were annealed in situ under UHV conditions at 850 °C for 15 minutes to remove the native oxide. The quality and/or the surface reconstruction of the surface were analyzed in situ by RHEED. Afterwards a thin layer of Au was deposited on the substrate at a T_S between 500 °C and 570 °C. After reaching T_S the Au deposition and then the Si deposition were immediately started. The thickness of the Au layer was varied between 0.5 nm and 4 nm. These experiments yielded an optimum T_S of 525 °C. Furthermore, at this T_S the highest density of Au droplets was received for a nominal Au layer thickness of 2 nm [25].

Droplets were formed by this procedur as demonstrated below. According to the Au–Si bulk phase diagram, a eutectic should be formed at about 360 °C. In our experiments we observed the formation of a liquid phase at about 280 °C.

To determine the morphology of the specimens, especially the growth behavior and the crystal structure of the NWs, the samples were analyzed ex situ by SEM, TEM and high-resolution transmission electron microscopy (HREM). Figure 1 represents a typical SEM image of the

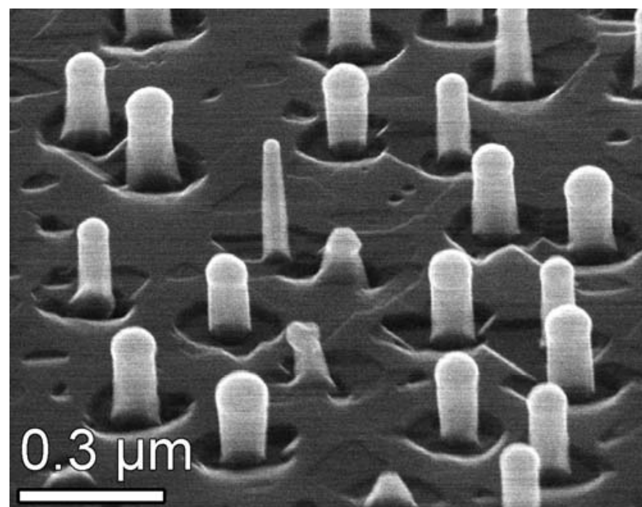

Fig. 1. SEM overview image of <111> oriented Si NW grown on a Si {111} substrate at T_S = 525 °C. The Au layer amounted to 2 nm, the growth time t_G = 120 min. Notice that for such SEM observations the samples were tilted and so the NWs appear to be shortened.

© 2006 Carl Hanser Verlag, Munich, Germany www.ijmr.de Not for use in internet or intranet sites. Not for electronic distribution.

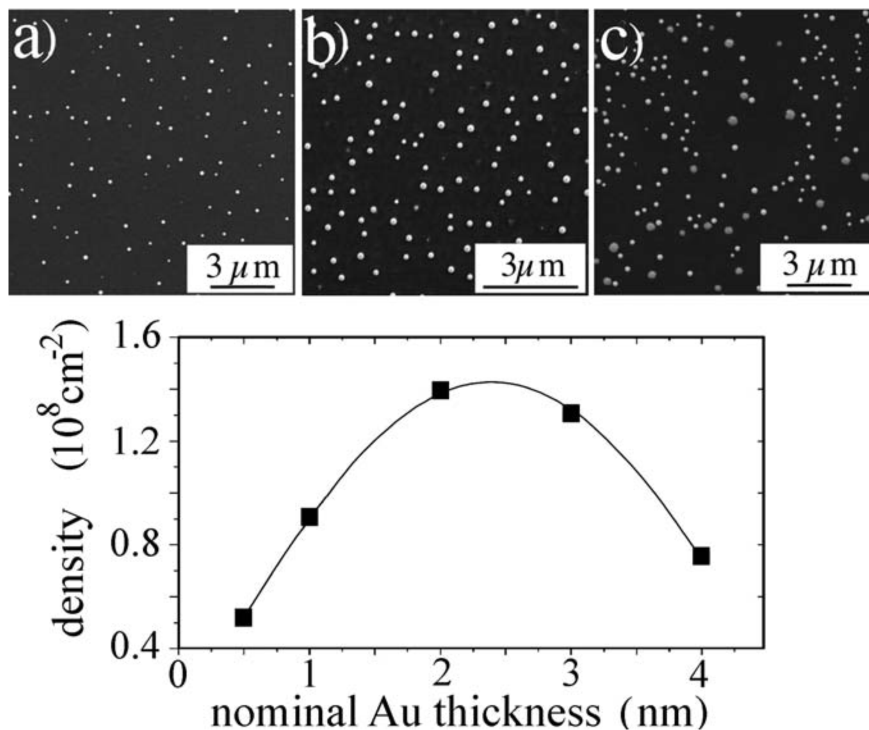

Fig. 2. Top-view SEM image of Au droplets/NWs. The nominal deposited Au layer thickness: (a) 0.5 nm, (b) 2 nm, and (c) 4 nm, respectively at T_S of 525 °C and t_G of 120 min. The optimum exists for a Au thickness of about 2 nm.

NWs. The nominal thickness of the Au layer needed to form droplets amounted to 2 nm, the growth time t_G amounted to 120 min. The NWs show a pillar shape. They are capped by Au droplets and stay in pits.

3. Results

3.1. Formation of the Au seed

For both CVD and MBE techniques, the Au droplets locally modify the interface energy and so generate favored places for the formation of NWs. Differing from the CVD technique, in the case of MBE we deal with a substrate surface that is clean and free of an oxide layer. For our experiments we used Au seeded substrates where the Au-droplets/NWs are characterized by a specific size distribution and density. This should allow the study of the influence of these parameters on the wire growth.

In a first set of experiments, we determined the optimum nominal thickness of the deposited Au layer that results in the highest density of droplets and subsequently grown NWs. Figure 2 presents top-view SEM images where the nominal deposited Au layer thickness was varied in the range from 0.5 nm to 4 nm. The Au layer and subsequently the Si were deposited at a substrate temperature of 525 °C for a growth time of 120 min. The largest density of NWs of 1.4×10^8 cm^{-2} was achieved for a nominal Au thickness of 2 nm (Fig. 2b). This is demonstrated by the density curve seen in the lower part of Fig. 2.

It has to be stated that, in general the Au droplets have a broad size distribution for all t_G and T_S ranging from 5 nm $< r <$ 300 nm, as confirmed by SEM.

Smaller droplets ($r <$ about 5 nm) could not be identified by SEM. The large droplets have a crystalline structure. The wire growth is initiated mainly by those Au dots with a size (radius) lying between approximately 30 and 150 nm.

In a second set of experiments we analyzed the influence of annealing on the radius r and the density of the clusters. The evolution of the cluster distribution can be characterized qualitatively as Ostwald ripening. As an example, Fig. 3 shows the changes of the droplet size distribution before and after a thermal anneal at 525 °C for 180 min, respectively. Figure 3a and c represent the related SEM images, where the size distributions (cluster radius r) are given as histograms (Fig. 3b and d). In this particular case the maximum of the distribution is changed from $r = 56$ nm to $r = 154$ nm. Furthermore, the droplet density is decreased by a factor of about 13. Quantitatively this Ostwald ripening can be described by a theory discussed in detail by Lifshitz, Slyozov and Wagner [26, 27] (LSW theory). Corresponding calculations are inserted as curves in Fig. 3b and d, respectively.

Beside this droplet formation, the whole {111} substrate surface is covered by a thin Au : Si layer. RHEED in-situ experiments in the MBE chamber demonstrated a transformation of the surface reconstruction from a (7×7) structure (typical for a clean Si surface) to a $(\sqrt{3} \times \sqrt{3})$ Au : Si structure during the beginning of Au deposition. In this respect we would like to refer to [28], where intensive investigations on the Au–Si {111} surface reconstruction are presented. By applying TEM/HREM investigations on cross-section samples, we noticed that the Au : Si modified surface has more a character of a “wetting layer”; its “thickness” < 0.5 nm [29]. We suppose that such a “wetting layer” is a continuous thin film and might play an important role in the surface diffusion of Au atoms and Si ad atoms. From the experiments, as an example at $T_S = 525$ °C and $t_G = 180$ min (Fig. 3c), we estimate a mean diffusion radius for Au atoms of about 650 nm. The existence of this “wetting layer” also becomes indirectly visible in TEM images as a fine decoration of small amorphous Au clusters (diameter < 2 nm) after cooling down the samples to RT: the continuous Au : Si layer segregates. These small Au clusters

© 2006 Carl Hanser Verlag, Munich, Germany www.ijmr.de Not for use in internet or intranet sites. Not for electronic distribution.

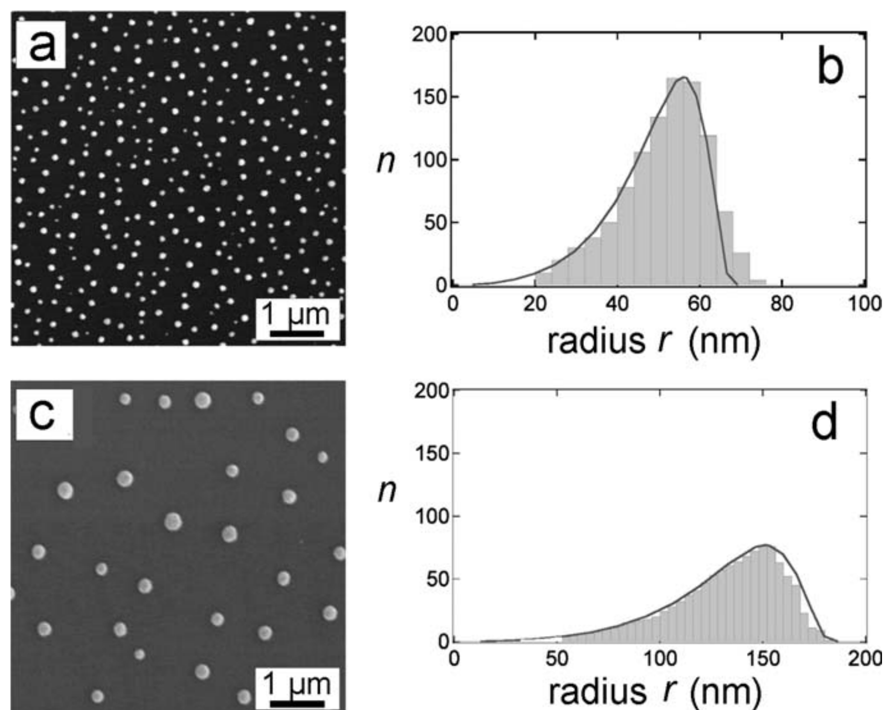

Fig. 3. Ostwald ripening of the Au droplets at 525 °C. (a) SEM micrograph of the droplets after the Au layer deposition, (c) after an annealing for 180 min. (b) and (d) represent the corresponding size distribution (radius *r*): bars – experimental data, curves – calculations concerning the LSW theory.

© 2006 Carl Hanser Verlag, Munich, Germany www.ijmr.de Not for use in internet or intranet sites. Not for electronic distribution.

are visible in TEM micrographs, such as in Fig. 4, not only for the substrate but also for the NW surface, and behave as a decoration of surface morphology.

3.2. Initial stage of Si NW growth

The initial stages of growing NWs are demonstrated in the cross-section TEM micrographs in Fig. 5. This shows the time development of the NWs after starting the Si flux from 0 min up to 45 min. In these TEM bright-field images the Au droplets are visible from their dark contrast. The six images correlate to six different growth experiments of different Si deposition times, where T_S was 525 °C in all of them. For an interpretation of the micrographs we have to consider that the samples represent the NWs after stopping the Si flux and an immediate fast cooling. Therefore, the TEM images might not correctly present the morphology of the growth front during growth. However, relevant conclusions can be drawn.

The {111} interfaces between the NWs and their Au droplets are flat. In particular, HREM micrographs demonstrate that the interface is mostly atomically flat. After specific growth times we could often observe the formation of small side walls visible at the outer rim (see, e. g., for 30 min and 45 min). We suppose that the droplets want to reduce their surface/interfaces during growth to minimize the system energy.

An unaffected Au cluster (0 min), which is formed by Au deposition on the hot surface shows a thin gray layer in the Si substrate just below the interface (Fig. 5, upper left). This might be caused by the formation of a Au : Si alloy according to the phase diagram. During cooling of the sample, the Si precipitates as a layer at the interface and includes some tiny Au crystals (nm range). As described in a former paper [29], Au can also form intrusions at the surfaces, which later can cause lattice defects in the growing Si layer.

From TEM and SEM micrographs we see that only those NWs with diameters between 40 nm and 300 nm grow. Droplets with larger diameters do not initiate a NW formation; they remain unaffected on the surface of the growing Si layer.

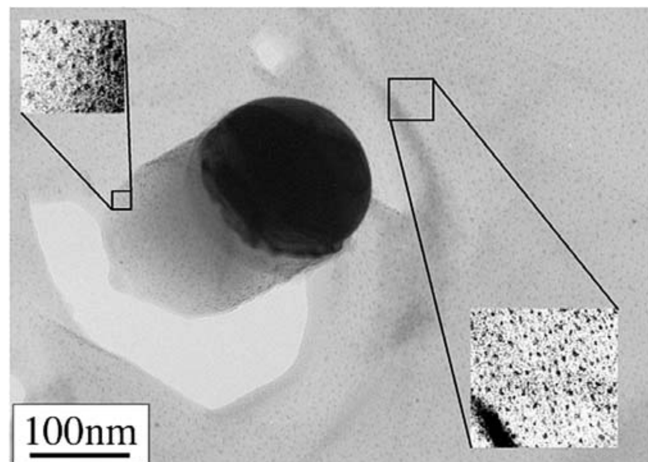

Fig. 4. TEM plan-view image of a Si NW with a Au droplet (black) at the tip. The inserts are magnified sections showing the fine Au decoration on the whole Si surface (right) as well as on the NW (left).

3.3. General aspects of the Si NW growth by MBE

In the following we will consider general aspects of the MBE growth of Si NWs resulting from our experiments, which will be briefly described. The main difference from other formation processes of NWs, e. g., by CVD, concerns the substrate surface, which allows the diffusion of adatoms. As mentioned above, Au atoms diffuse on the substrate surface with a relatively large diffusion coefficient resulting in a continuously ongoing ripening of the droplets at the top of the NWs. More important is that the Si adatoms impinging on the surface are not desorbed, but diffuse on

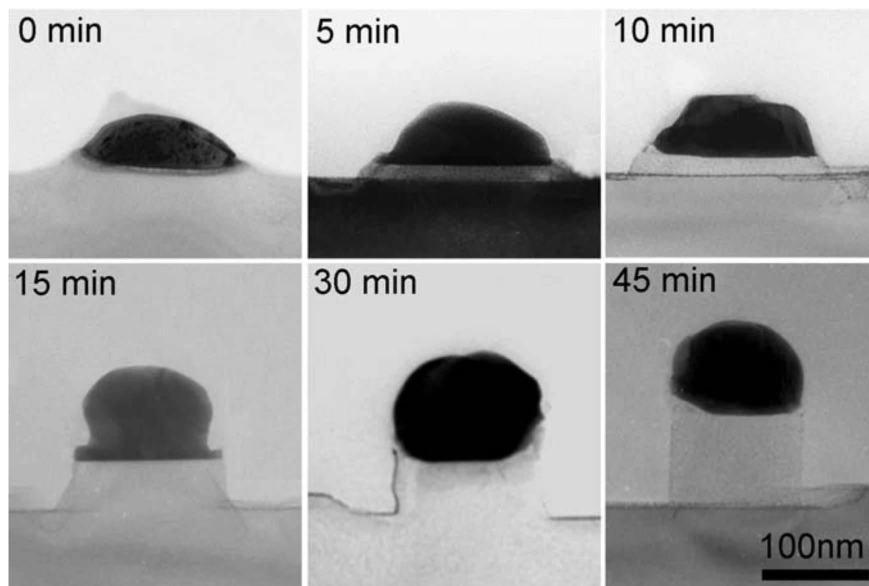

Fig. 5. TEM cross-section images of the first stages of the formation of Si NWs, where the droplets at the tip are visible by their dark contrast.

the substrate and then are incorporated in the growing Si layer. In that case one would assume that the NW and the Si layer grow with the same speed and no wire can be formed. However, adatoms in the proximity of a NW also diffuse towards and along the NW. This is caused by a concentration gradient since the concentration of adatoms drastically decreases at the liquid–solid interface (LS), where they are incorporated. Therefore, the growth of a NW results from the incorporation of two fluxes of Si adatoms, which is schematically demonstrated in Fig. 6a. There is a flux I_1 resulting from the direct impingement of Si atoms at the droplet and a subsequent diffusion to the reaction interface (LS interface) and a flux I_2 diffusing from the surrounding surface. TEM and SEM micrographs show that the NWs grow somewhat faster than the conventional Si layer. In the case of T_S of 525 °C the growth ratio L/L_l amounts to a mean value of 0.6. This value does not change in the temperature interval investigated. This behavior has already been discussed in a previous paper [24].

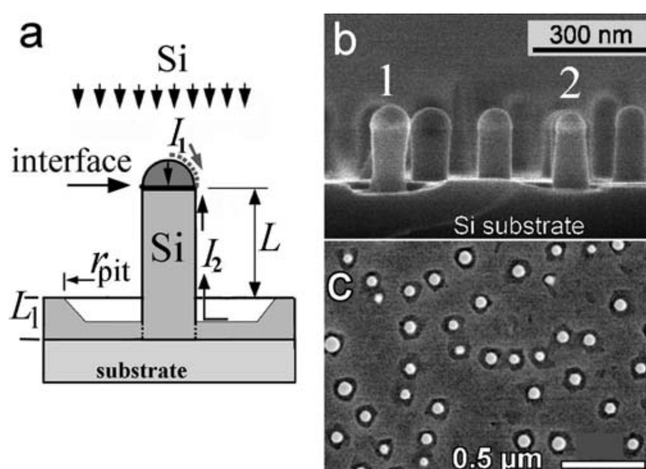

Fig. 6. (a) Schematic diagram of the growth geometry of a NW. The formation of a NW by two adatom fluxes I_1 and I_2 is always accompanied by the growth of a Si layer L_l. The cross-section SEM image (b) (t_G = 120 min) as well the plan-view SEM image (c) (t_G = 300 min) demonstrate that each NW stands in a pit resulting from Si consumption. T_S = 525 °C.

Furthermore, there are pits around the NWs with a radius r_{pit} similar to the diameter of the NW, as can be seen in the SEM images of Fig. 6b and c. We suppose that this material is also consumed by the NW and is included in the flux I_2. Figure 6b presents a cross-section of a sample showing the morphology of wires after a growth time of 120 min. For larger growth times a facetting of the wires is observed and the NW gets a quasi-sixfold symmetry (see also Fig. 10). This will be described below. Furthermore, the morphology of the pits is transferred to a triangular/tetrahedral one.

The wires mostly have a cylindrical shape (in the region of T_S = 525 °C) with a hemispherical Au cap and have diameters below 100 nm. They stand in a pit visible as a darker ring around them (Fig. 6c). The NW growth could be achieved only on <111> Si substrates. It has to be mentioned that in our MBE experiments we succeeded in growing only <111> oriented NW.

3.5. Ostwald ripening of Si NWs

In some cases we observed in SEM micrographs a slightly conical shape to the wires, i. e., a slight increasing (1) or shrinking (2) of the wire diameters with the growth time, as seen in Fig. 6b. This is related to the Ostwald ripening of the droplets, which continues during the first period of NW growth. This is more quantitatively visible in the top-view SEM image of Fig. 7 (upper row), where the wires are visible by their Au caps. As with the ripening of pure droplets (Fig. 3), the NW distribution/density is modified as well, as seen in the size distributions in the lower row for growth times of 0 min, 5 min, and 15 min. However, in this situation, some of the small NWs disappear, whereas others are growing. The peak of the experimental size distribution (bars) shifts from radius r = 56 nm to r = 64 nm within the first 15 minutes of growth. Small NWs disappear in such a way that, at first, the Au droplet is dissolved by ripening. The remaining “naked” NWs are transformed into needles with a tip radius of about 25 to 30 nm. Smaller tips were not observed, presumably this radius represents the stable minimum (Gibbs–Thomson effect). These Si

© 2006 Carl Hanser Verlag, Munich, Germany www.ijmr.de Not for use in internet or intranet sites. Not for electronic distribution.

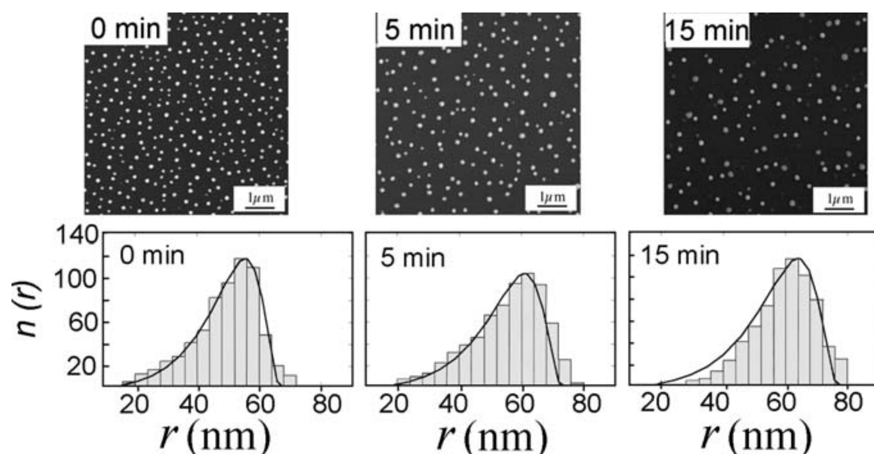

Fig. 7. SEM images confirm further Ostwald ripening during the first 15 min of NW growth. Upper row: top-view SEM image of the initial stage of NWs. The lower row presents the size distribution (r – NW radius) as histograms. The superimposed curves result from LSW simulations.

needles/NWs do not grow any more, and were later embedded in the growing Si layer.

The drastic decrease of the NW density at the beginning of growth is also demonstrated by Fig. 8. It shows the density as a function of the growth time for two T_S of 525 °C and 545 °C. After a t_G of about 120 min the density reaches a nearly constant value.

3.6. NW morphology as a function of T_S and t_G

The dependence of the growth time t_G and of the substrate temperature T_S on the NW growth will now be described. For the corresponding experiments the Au seeding conditions as well as the Si flux were kept constant. As an example, Fig. 9 shows NW growth as a function of three growth times t_G at T_S = 525 °C and T_S = 545 °C. Initial analysis of the SEM micrographs demonstrates that the lengths of the NWs grow linearly with t_G. This holds up to t_G = 240 min when the wires reach a length of approximately 0.5 μm (temperature dependent). For longer times the growth speed decreases, which indicates a limiting effect of the diffusion component I_2 on the growth. Second, NWs grown at higher T_S show larger diameters as well as larger lengths than those grown at lower T_S.

As a final result the morphology will be discussed for those NWs grown at longer times (t_G > 200 min). At first, the cylindrical shape is converted into a facetted one and its cross-section is transferred to a quasi-6-fold symmetry. This situation is demonstrated in Fig. 10, which shows a SEM image of a NW for t_G = 240 min. Starting from the base, the circular surface is converted into six {112} planes as marked. Furthermore these main side-facets contain smaller sub-facets. From TEM image analysis it follows that most of them have {111} surface planes, especially after longer growth. This morphology represents a possible state closer to thermodynamic equilibrium. The insert in the middle shows a top-view TEM micrograph of a NW without the Au droplet. This image demonstrates, first, the quasi-6-fold symmetry of the cross-section and, second, the existence of a lattice strain with a 3-fold symmetry visible by dark lines. These internal strain fields and related lattice-strain release within NWs will be discussed in more detail elsewhere.

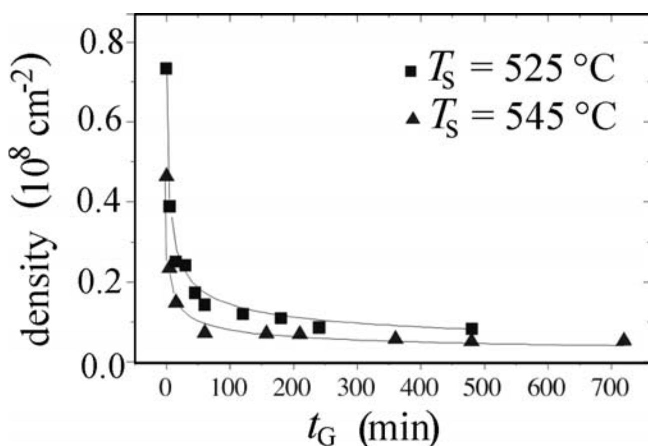

Fig. 8. The density of NWs versus the growth time t_G at two different growth temperatures T_S. The NW density decreases drastically during the first 30 min by Ostwald ripening and NW dissolution.

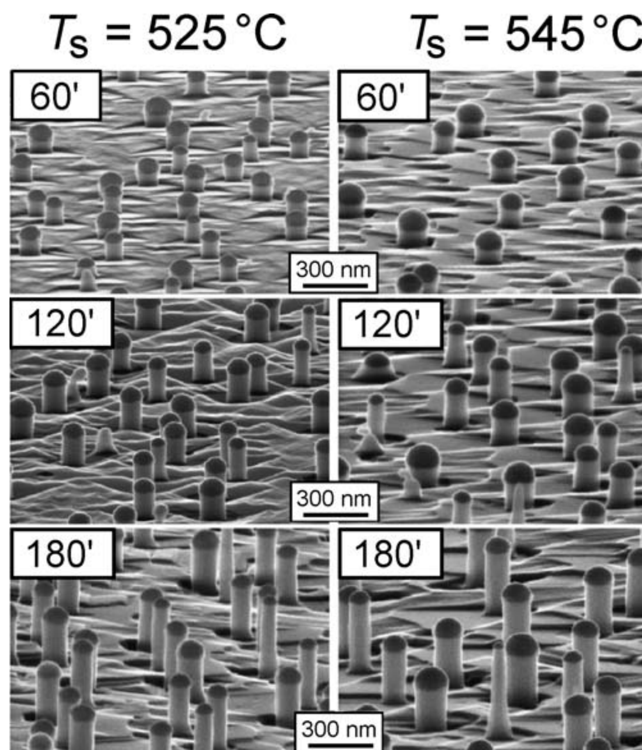

Fig. 9. Si NWs grown for 60 min, 120 min, and 180 min at T_S = 525 °C (left) and T_S = 545 °C (right).

© 2006 Carl Hanser Verlag, Munich, Germany www.ijmr.de Not for use in internet or intranet sites. Not for electronic distribution.

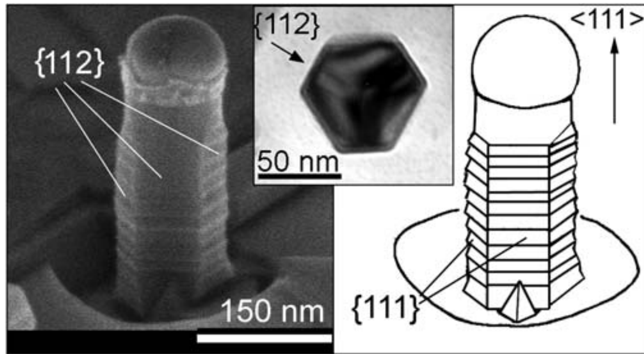

Fig. 10. Right: Morphology of an Si NW grown for 240 min. It has a quasi-6-fold cross-section with {112} main facets visible in TEM cross-section images (inserted in the middle). The small sub-facets have {111} surfaces planes schematically drawn in the right.

4. Discussion and conclusions

In general, our MBE growth experiments yielded the following results. Free-standing Si NWs were generated on {111} Si substrates within a temperature range of 475 °C to 570 °C at a constant Si flux rate of 0.05 nm s^{-1}. They are always <111> epitaxially oriented. No other NW orientations could be achieved on a clean substrate surface, and no other Si substrate surface orientations besides {111} could be activated. The Au seed was optimized to produce droplet diameters between 40 nm and 500 nm. The NW growth proceeds only for droplet diameters between 70 nm and 300 nm, and the NW diameters correlate to the Au droplets. NW lengths up to about 0.6 μm could be achieved at 525 °C. The shape of the NWs is characterized by a cylindrical pillar for growth time up to about 180 min.

The generation of Si NWs by MBE under UHV conditions shows significant differences to other growth methods, such as CVD. This was found for the thermodynamic behavior as well as for the kinetics of the formation process.

First, this concerns the initiation of the NW growth by the Au droplets. These droplets do not act as a catalyst for a precursor gas, but result in a liquid Si/Au eutectic phase formation considerably reducing the nucleation barrier for whisker growth. A supersaturation is supplied by the difference of the chemical potential of Si atoms located in the overgrown layer and on the top of the whisker. It appears due to relaxation of elastic energy stored in overgrown layer caused by gold intrusions. The resulting size of the droplet determines the diameter of the growing NW. The Si supersaturation generated in the droplet causes a precipitation at the liquid-solid (LS) interface by {111} step flow – a pillar is created at such places. This can also be regarded as a liquid-phase epitaxy. In the case of MBE grown NWs we have additional hints from TEM and HREM that the pillars are characterized by a radial lattice strain field (see also insert of Fig. 10), especially with a 3-fold symmetry in the growth direction. We assume that the corresponding radial stresses are caused by the incorporation of point defects, presumably Au atoms. The existence of point defects was also concluded from the formation of defects in NW regions after irradiating the samples in the TEM (defect-free crystal regions remained stable under the electron-beam). Post-growth oxidation as a reason for high stress in nanostructures seems to us unlikely. As already discussed by the authors [29], a lattice strain was detected in the base region of the NWs, whereas the upper part is strain relaxed. Therefore, the formation of NWs has thermodynamic similarities to the formation of islands via the Stranski–Krastanow growth mode (strain-driven mechanism of NW growth [29]).

Second, with regard to kinetic aspects, the NWs are formed by two components of material flow. Beside the flux of adatoms collected by the droplet at the tip (I_1), a significant amount of Si ad-atoms diffuse from the surrounding substrate surface to the {111} Si/Au interface – the place of adatom incorporation into the droplet. The Si lattice growth seems to proceed via the fast flow of {111} steps on the {111} growth surface; the adatoms have to diffuse to the corresponding steps where they are incorporated into the crystal lattice. The steps are created at the periphery of the growth surface sometimes forming a rim (see, e. g., Fig. 5 – 30 min). The HREM micrographs show mono-atomic flat LS interfaces; we had no indication of two-dimensional nucleation.

Furthermore, the “Au wetting layer” on the surfaces has an influence on the kinetics. It seems to influence not just the diffusion of Au atoms. Of more importance is that it increases the surface diffusion of the Si adatoms – a precurser to NW formation.

In SEM micrographs we observed that Au droplets with diameters > 300 nm do not initiate NW formation but stay unaffected on the growing surface. We suppose that for such large droplets the difference of the chemical potentials is not large enough for any additional Si atom incorporation. Si whiskers with a diameter below 40 nm do not grow, most likely due to the Gibbs–Thomson effect. If the Au droplets decrease to a certain/critical radius during further Ostwald ripening, they may even be dissolved. The remaining small NWs will subsequently be partly dissolved or embedded in the growing Si layer.

During the first period of growth we observe a linear increase of the NW length with time. Later, for NW lengths above a specific length (about 0.5 μm in our experiments, T_S dependent) we observe a slow-down of the growth, which we explain by a diffusion-limited process.

In contrast to the CVD growth process, in the MBE experiments described here the NWs with smaller diameters grow faster than the thicker ones (length $l \propto 1/r$). This phenomenon is caused by the additional surface diffusion of Si adatoms (component I_2). The growth rate is thereby determined by the ratio between the NW surface ($\propto r^2$) to its volume changes ($\propto r^3$). The specific aspect ratio (length/radius), of course, depends on the chosen temperature T_S.

With regard to their technological application, such free-standing pillars can be arranged in defined patterns by using lithographic methods, e. g., by nanosphere lithography [30].

The authors would like to thank A. Frommfeld for the support of the MBE experiments, F. Syrowatka and S. Hofmann for SEM analysis, S. Hopfe for TEM specimen preparation, and M. Werner for specific TEM analysis. The author L. Schubert appreciates the financial support of the Deutsche Forschungsgemeinschaft (Graduierten-Kolleg). The work was also partly supported by European project NODE (FP6/ 015783).

© 2006 Carl Hanser Verlag, Munich, Germany www.ijmr.de Not for use in internet or intranet sites. Not for electronic distribution.

References

[1] Y. Nakajiama, Y. Takahashi, S. Horiguchi, K. Iwadate, H. Namatsu, K. Kurihara, M. Tabe: Appl. Phys. Lett. 65 (1994) 2833.
[2] N. Usami, T. Mine, S. Fukatsu, Y. Shiraki: Appl. Phys. Lett. 64 (1994) 1126.
[3] J.L. Liu, Y. Shi, F. Wang, Y. Lu, R. Zhang, P. Han, S.L. Gu, Y.D. Zheng: Appl. Phys. Lett. 68 (1996) 352.
[4] C.M. Lieber: MRS Bulletin 28 (2003) 128.
[5] R.S. Wagner, W.C. Ellis, K. Jackson, S.M. Arnold: J. Appl. Phys. 35 (1964) 2993.
[6] R.S. Wagner, W.C. Ellis: Transaction of the Metallurgical Society of AIME 233 (1965) 1053.
[7] E.I. Givargizov: J. Cryst. Growth 31 (1975) 20.
[8] R.S. Wagner a, W.C. Ellis: Appl. Phys. Lett. 4 (1964) 89.
[9] Y. Cui, L.J. Lauhon, M. Gudiksen, J. Wang, C.M. Lieber: Appl. Phys. Lett. 78 (2001) 2214.
[10] J. Westwater, D.P. Gosain, S. Tomiya, S. Usui: J. Vac. Sci. Technol. B 15 (1997) 554.
[11] Y. Wu, Y. Cui, L. Huynh, C.J. Barrelet, D.C. Bell, C.M. Lieber: Nano Lett. 4 (2004) 433.
[12] J. Westwater, D.P. Gosain, S. Usui: Phys. Stat. Sol. A 165 (1998) 37.
[13] Q. Tang, X. Liu, T.I. Kamins, G.S. Salomon, J.S. Harris: Appl. Phys. Lett. 81 (2002) 2451.
[14] J.L. Liu, S.J. Cai, G.L. Jin, Y.S. Tang, K.L. Wang: Supp. Microstr. 25 (1999) 477.
[15] P. Finnie, Y. Homma: J. Cryst. Growth 201/202 (1999) 604.
[16] J.L. Liu, S.J. Cai, G.L. Jin, S.G. Thomas, K.L. Wang: J. Cryst. Growth 200, (1999) 106.
[17] Y-H. Yang, S.-J Wu, H.-S. Chiu, P.-I. Lin, Y.-T. Chen: J. Phys. Chem. B 108, 846 (2004)
[18] F.M. Kolb, H. Hofmeister, R. Scholz, M. Zacharias, U. Gösele, D.D. Ma, S.T. Lee: J. Electrochem. Soc. 151 (2004) 375.
[19] M. Borgström, K. Deppert, L. Samuelson, W. Seifert: J. Cryst. Growth 260 (2004) 18.
[20] T. Martenson, M. Borgström, W. Seifert, B.J. Ohlsson, L. Samuelson: Nanotechn. 14 (2003) 1255.
[21] H.D. Park, T.P. Hogan: J. Vac. Soc. Technol. B 22 (2004) 237.
[22] Z.H. Wu, X.Y. Mei, D. Kim, M. Blumin, H.E. Ruda: Appl. Phys. Lett. 81 (2002) 5177.
[23] F.M. Ross, J. Tersoff, M.C. Reuter: Phys. Rev. Lett. 95 (2005) 146104.
[24] L. Schubert, P. Werner, N.D. Zakharov, G. Gerth, F. Kolb, L. Long, U. Gösele, T.Y. Tan: Appl. Phys. Lett. 84 (2004) 4968.
[25] L. Schubert, N.D. Zakharov, G. Gerth, H.S. Leipner, P. Werner, U. Gösele: Proc. DPG Meeting, Berlin 2005.
[26] I.M. Lifshitz, V.V. Slyozov: J. Phys. Chem. Solids 19 (1961) 35.
[27] C. Wagner: Zeitschrift für Elektrochemie 65 (1961) 581.
[28] S. Ino: Reflection High-Energy Electron Diffraction and Reflection Electron Imaging of Surfaces, NATO ASI Series B, Plenum Press, New York (1988).
[29] N.D. Zakharov, P. Werner, G. Gerth, L. Schubert, L. Sokolov, U. Gösele: J. Cryst. Growth 290 (2006) 6.
[30] B. Fuhrmann, H.S. Leipner, H.-R. Höche, L. Schubert, P. Werner, U. Gösele: Nano Lett. 5 (2005) 2524.

(Received January 16, 2006; accepted April 22, 2006)

Correspondence address

Dr. Peter Werner
Max Planck Institute of Microstructure Physics
Weinberg 2, D-06120 Halle (Saale), Germany
Tel: +49 345 5582629
E-mail: werner@mpi-halle.de

You will find the article and additional material by entering the document number MK101332 on our website at www.ijmr.de

© 2006 Carl Hanser Verlag, Munich, Germany www.ijmr.de Not for use in internet or intranet sites. Not for electronic distribution.